Featured in Physics

Isotope ratio dual-comb spectrometer

Alexandre Parriaux [1,*] Kamal Hammani [1] Christophe Thomazo [2,3] Olivier Musset [1] and Guy Millot [1,3]

[1]*Laboratoire Interdisciplinaire Carnot de Bourgogne, CNRS UMR 6303, Université Bourgogne Franche-Comté, 9 avenue Alain Savary 21000 Dijon, France*

[2]*Biogéosciences, CNRS UMR 6282, Université Bourgogne Franche-Comté, 6 boulevard Gabriel 21000 Dijon, France*

[3]*Institut Universitaire de France, 1 Rue Descartes 75005 Paris, France*

(Received 4 March 2022; revised 30 March 2022; accepted 4 April 2022; published 5 May 2022)

We demonstrate the use of dual-comb spectroscopy for isotope ratio measurements. We show that the analysis spectral range of a free-running near-infrared dual-comb spectrometer can be extended to the midinfrared by difference frequency generation to target specific spectral regions suitable for such measurements and especially the relative isotopic ratio $\delta\,^{13}C$. The measurements performed present very good repeatability over several days with a standard deviation below 2‰ for a recording time of a few tens of seconds, and the results are compatible with measurements obtained using an isotope ratio mass spectrometer. Our setup also shows the possibility to target several chemical species without any major modification, which can be used to measure other isotopic ratios. Further improvements could decrease the uncertainties of the measurements, and the spectrometer could thus compete with isotope ratio spectrometers currently available on the market.

DOI: 10.1103/PhysRevResearch.4.023098

I. INTRODUCTION

Isotope ratio measurement (IRM) is a widely used technique that shows great interest for a large range of applications. For instance, strontium ratio $^{87}Sr\,/\,^{86}Sr$ analyses were successfully used to reconstruct the Egtved Girl's life that occurred 3500 years ago [1]. Still related to chronological dating, measurements of the oxygen ratio $^{18}O\,/\,^{16}O$, carbon ratio $^{13}C\,/\,^{12}C$, and thorium ratio $^{230}Th\,/\,^{232}Th$ ratio have been used for the dating of prehistoric human constructions such as the Bruniquel Cave [2]. In astronomy, IRMs allow the study of the atmosphere and sedimentary rocks of other planets, such as Mars [3–5], or to investigate the composition of meteorites by analyzing magnesium or oxygen isotopes [6,7]. In more daily life-related applications, food and beverages can be subjected to IRMs [8], such as for testing ingredients in beers [9] or for detecting the geographical origin of wines [10,11], mushrooms [12], and even cheeses [13]. Another example of application where IRMs are performed is the medical domain such as for the detection of *Helicobacter pylori* infection, which can be done by measuring the carbon ratio $^{13}C\,/\,^{12}C$ out of the exhaled air of a patient [14].

All the examples presented above mostly use a mass spectrometer for IRMs, which is a specific high-performance instrument but costly and with measurement times that can be of several minutes. Moreover, the samples under study might need to be pretreated before being analyzed which increases the complexity and can induce more uncertainties [15]. Hence other techniques for IRMs have been developed, and absorption spectroscopy is one of them when studying gases. This nondestructive technique presents the advantage of being based on optics and lasers which gives an instrument smaller in size and capable of being used for on-field measurements [16]. Direct absorption [17], frequency modulation [18], or cavity ring-down spectroscopy [19] are generally used for these measurements. However, in the field of absorption spectroscopy, new techniques have also been developed in recent years such as dual-comb spectroscopy (DCS) [20–22]. DCS shows several characteristics such as a high spectral resolution, no mobile parts in the setup, and the potential to perform real-time analyses. These features are very interesting for IRMs in gases and to the best of our knowledge only a few works have considered the use of DCS for this application [23,24], but no quantitative measurements were performed.

In this paper, we present the use of DCS for IRMs and we demonstrate the feasibility of the technique by measuring the relative carbon isotopic ratio $\delta\,^{13}C$ of gas samples. First we describe the DCS method and the experimental setup considered here. Then we will see some examples of absorption spectra that can be recorded with our setup to illustrate its features. After that we will present and show how IRMs can be performed with our DCS setup by taking the example of carbon dioxide for $\delta\,^{13}C$ measurements. In addition, we will show that the frequency tunability of our setup can be used to target other chemical species for IRMs and especially nitrous oxide for nitrogen isotopes studies. Finally, we will discuss our results and potential enhancements that could be done in future works to improve the use of the DCS technique for IRMs with a higher accuracy and a lower uncertainty.

*Corresponding author: alexandre.parriaux@u-bourgogne.fr; Current address: Laboratoire Temps-Fréquence, Institut de Physique, Université de Neuchâtel, Avenue de Bellevaux 51, 2000 Neuchâtel, Switzerland.

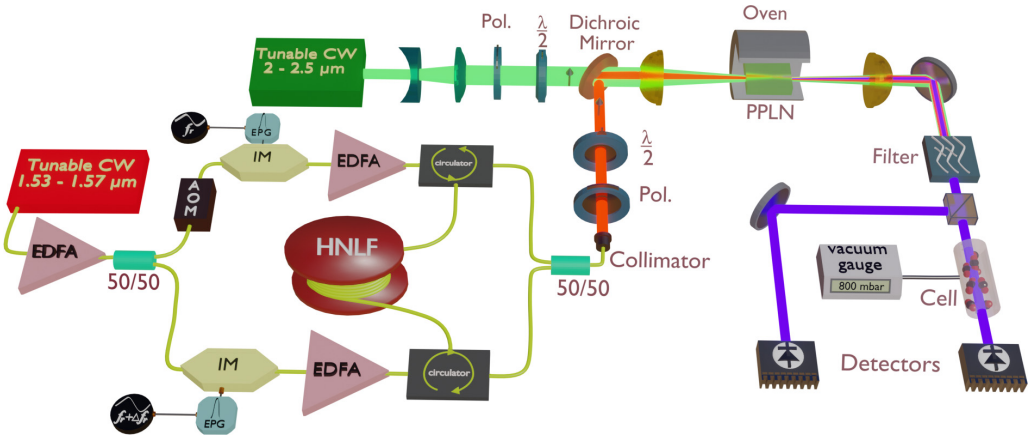

FIG. 1. Schematic showing the MIR dual-comb spectrometer based on the difference frequency conversion of combs generated by electro-optic modulators around 1.55 μm. CW, continuous wave; EPG, electrical pulse generator; EDFA, erbium doped fiber amplifier; AOM, acousto-optic modulator; IM, intensity modulator; HNLF, highly nonlinear fiber.

II. MIDINFRARED ELECTRO-OPTIC DUAL-COMB SETUP

Spectroscopic applications can be performed using several techniques, but DCS has been shown to be highly suitable for high-resolution spectral measurements and short-time acquisitions. This technique, which is based on the study of the interference between two mutually coherent frequency combs with slightly different repetition frequencies, has been intensively studied and refined in the past years [20–22]. The Fourier transform of the interference time signal, which is called the interferogram, is also a comb but with a line spacing that is the difference of the repetition frequencies of the combs and with a central frequency that lies in the radio-frequency (RF) domain. When at least one of the optical combs passes through a gas sample, the absorption feature of the gas will be seen in the optical domain but also in the RF domain, which makes it much easier and straightforward to detect by using only a low bandwidth photodetector and an oscilloscope. Since the repetition frequency of the combs can easily be around a few hundreds of MHz, using the technique for gas analysis enables high-resolution spectroscopic applications.

Lots of experimental setups have been designed for DCS, but here we use a setup based on electro-optic modulators [25]. This setup, whose architecture is presented in detail in Ref. [26], shows particular advantages for DCS since there is no need of locking between the combs which drastically simplifies the technique [25,26]. However, in its basic design [26], the setup operates around 1.55 μm, which is not really suitable for spectroscopic applications. Indeed, most molecules do not show strong absorption features in this spectral region; thus long absorption cells are required to perform DCS, which can be cumbersome. To bypass this problem, the working spectral region of the setup can be extended to the midinfrared (MIR) region where molecular absorptions are much stronger than at 1.55 μm [27]. In our case, we use difference frequency generation (DFG) in a periodic poled lithium niobate (PPLN) crystal to reach the spectral region between 4.2 and 4.85 μm. The experimental setup and its spectral extension part to reach the MIR is presented in Fig. 1.

The dual-comb spectrometer can be divided into two parts. The first is the generation of frequency combs at 1.55 μm as described in Ref. [26], and the second part is the frequency conversion of the previous combs in the MIR using DFG. Regarding the part at 1.55 μm, we start with a continuous-wave (CW) laser at 1.55 μm that is amplified up to 150 mW. The CW is then split in two arms that are both intensity modulated using electro-optic modulators, which produce 40 GHz wide frequency combs with a cardinal sine shape. The intensity modulators are driven by electrical pulse generators which operate by the control of sinusoidal wave form generators that set the repetition frequency of the combs to $f_r = 250$ MHz and $f_r + \Delta f_r = 250.025$ MHz. Note that prior to the modulation, one of the arms is frequency shifted by 40 MHz using an acousto-optic modulator to prevent aliasing in the later detection. After generating combs, both arms are amplified up to a peak power of 26 W and sent counterpropagatively in a 800-m-long highly nonlinear fiber of dispersion $D = -91$ ps.nm^{-1}.km^{-1}, linear loss $\alpha = 0.55$ dB.km^{-1}, and Kerr coefficient $\gamma = 4.6$ W^{-1}.km^{-1} at 1.55 μm. This fiber was chosen to obtain a spectral broadening as high as possible and a flat-topped shape by dispersive shock waves [26–28], giving us spectra that are 3 nm wide.

After spectral broadening, both combs are mixed with a 50/50 combiner and sent to free space using a fibered collimator. Using a dichroic mirror, the combs with a peak power of 1.4 W are then combined with an idler wave consisting of a wavelength tunable CW laser from 2 to 2.5 μm whose power can be set up to 5 W. The beam is then focused on a 10-mm-long temperature-controlled commercially available PPLN crystal (Covesion) for DFG. Note that the polarization of the combs and the idler wave are controlled with polarizers and half wave plates to be aligned with the dipole moment of the crystal, which is needed to achieve the highest DFG efficiency. Also note that by modifying appropriately the wavelength of the idler, the temperature, and the poling period of the PPLN crystal, the central wavelength of the MIR signal can cover the range 4.2 to 4.85 μm. Here we choose to convert both combs in a single crystal which shows a certain ease of doing [29], but note that the combs could be converted individually, which would enable the possibility to perform dispersion spectroscopy [27,30]. At the output of the crystal, the beam is collimated and filtered to keep only the MIR part. A 50/50 beamsplitter is then used to split the MIR signal in

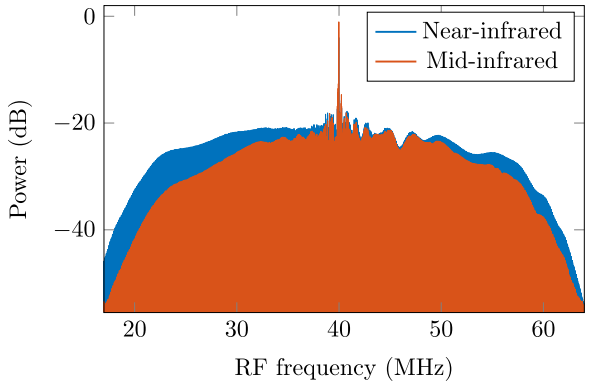

FIG. 2. Comparison of the RF combs obtained by the beating of the near-infrared (blue) and MIR (red) combs. The bandwidth difference is due to the finite spectral acceptance of the crystal used for difference frequency generation in the MIR.

two parts, providing a signal and a reference arm which are both ending with a photovoltaic detector (Vigo) for acquiring the dual-comb interferograms. The signal arm is composed of a pressure-monitored cell that can be filled with various gases.

We recorded an interferogram of 80 ms that is Fourier transformed to reveal the RF comb made of the beating between the MIR combs. This RF comb is compared with the one we obtained at 1.55 μm under similar conditions and both of them are presented in Fig. 2. We can observe that the RF comb resulting from the MIR beating is slightly narrower than the RF comb resulting from the near-infrared beating, which is due to the spectral acceptance bandwidth of the PPLN crystal. But besides that, both RF combs are highly similar and possess a signal-to-noise ratio of 35 dB.

III. SPECTROSCOPIC APPLICATIONS

A. Absorption spectroscopy

Since MIR combs are generated, spectroscopy can be performed. First, we set the wavelength of the near-infrared combs to 1555 nm and the idler wave to 2373 nm, giving us a MIR signal around 4511 nm. We use a 5-cm-long cell that is filled with a CO_2 gas sample made of 99% of $^{13}CO_2$ at a total pressure of 173 mbar, and we record at the same time two 10-s-long interferograms, one for the reference arm and one for the signal arm. Both are divided into 80-ms subinterferograms, Fourier transformed, and averaged to obtain the reference and signal RF combs. The envelope of the resulted combs is extracted and compared for baseline correction, which gives us the transmission spectrum of the sample in the cell that is presented in Fig. 3 (top). The frequency scale of the spectrum is converted back in the optical domain using the parameters of our setup and the relation between the RF and optical domains. In the following, the same procedure will be performed to obtain the transmission spectrum of other gas samples under study.

Once the transmission spectrum is obtained, we compared it with a fitted spectrum based on the least-squares regression of a set of Voigt profiles with line parameters given by the HITRAN database [31,32]. For the regression, the isotopic ratios $^{13}r = {}^{13}\mathrm{C}/{}^{12}\mathrm{C}$ and $^{18}r = {}^{18}\mathrm{O}/{}^{16}\mathrm{O}$ are taken as free parameters. Since we are not referencing any of the CW lasers we use, we also take into account a small shift for recentering the spectrum relatively to the rough frequency value expected by the DFG process. We also consider a baseline correction of the absorption spectrum since the comparison between the reference and the signal arm is not perfect. The obtained fitted spectrum is shown in Fig. 3 (middle) and the difference with the experimental data is presented in Fig. 3 (bottom) showing a very good agreement.

Due to the gas chosen for this experiment and the spectral region investigated, Fig. 3 shows several lines coming from different isotopologues where some of them are highlighted. With this simple example, one can imagine that the data obtained from the comparison between the experimental and the fitted spectra can be used to extract isotopic ratios such as here, ^{13}r, or ^{18}r and thus perform IRMs.

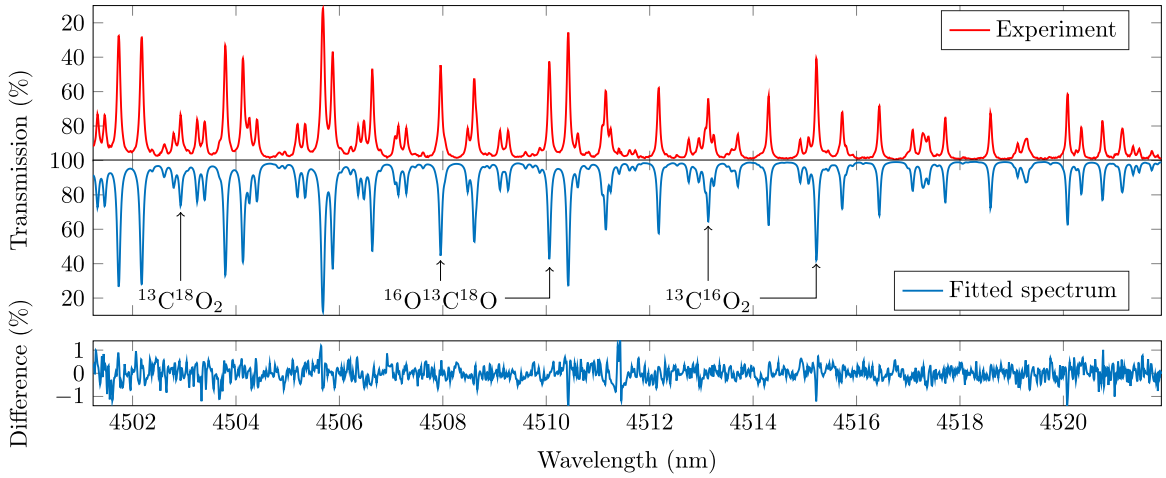

FIG. 3. (Top) Absorption spectrum of a CO_2 gas sample made of 99% of $^{13}CO_2$ recorded around 4511 nm at a pressure of 173 mbar using a 10-s-long interferogram. (Middle) Fitted absorption spectrum using line parameters coming from the HITRAN database. (Bottom) Difference between the experimental and fitted spectra.

B. IRMs

The basic idea for IRMs using absorption spectroscopy is to target a spectral region where the setup can record the absorption features of several isotopologues. In our case, and compared with the last spectrum we presented, we will be more restrictive since we will focus on particular regions where the isotopologues show absorption lines of similar intensities at an isotopic abundance close to the natural one. This is done to avoid lines that saturate, which could deteriorate the data analysis but also because most of IRMs find values that are close to the natural isotopic abundance. Note that other kinds of restrictions could be considered [33]. First, let us consider carbon dioxide and its $^{13}C\,/\,^{12}C$ ratio.

1. Carbon dioxide and $\delta\,^{13}C$

The ratio $^{13}r = {}^{13}C\,/\,{}^{12}C$ can be studied for carbon dioxide by analyzing the spectral region around $4.36\,\mu$m, which mainly shows absorption lines coming from the ν_3 band of $^{12}CO_2$ and $^{13}CO_2$ at similar intensities when these isotopologues are close to the natural isotopic abundance. This spectral region is also chosen since it has the advantage of not showing strong water absorption lines, which could deteriorate our measurements. In our case, we target the spectral region roughly between 4355 and 4373 nm. Then, we fill a 10-cm-long cell with a gas mixture of carbon dioxide and synthetic air (the partial pressures will be detailed later) and we record the transmission spectrum of the sample. The experimental spectrum is then compared with a fitted spectrum in the same way as explained before and with free parameters that are the ratios ^{13}r, ^{18}r, the partial pressure of carbon dioxide p_{CO_2}, a global frequency shift of the spectrum, and a function to correct the nonperfect baseline.

From the comparison between the experimental data and the fitted spectrum, one can extract the isotopic ratio ^{13}r given by the least-squares regression. However, this way of doing it will give us an absolute measurement, which is generally very complex to perform accurately since a lot of phenomena can induce systematic errors [15,34]. Nevertheless, it is generally possible to significantly bypass this issue by measuring a relative isotopic ratio rather than an absolute one. By using a reference sample that is precharacterized in isotopic ratio $^{13}r_{\text{ref}}$, one can measure the relative value between an unknown sample of isotopic ratio $^{13}r_{\text{exp}}$ and the one that is precharacterized. The relative value is usually expressed using the δ notation in ‰ which is, in the case of ^{13}C and ^{12}C, defined as

$$\delta\,^{13}C = 1000\left(\frac{^{13}r_{\text{exp}}}{^{13}r_{\text{ref}}} - 1\right)‰ \quad . \tag{1}$$

In the case of the ^{13}r ratio measurement, the reference sample is usually related to the Vienna Pee Dee Belemnite (VPDB) [35]. Note that absolute measurements are possible, but they require much more complex setups and are usually used for highly precise measurements [36]. To summarize, an isotope ratio spectrometer needs to be calibrated.

Several calibration procedures are reported in the literature and a practical guide can be found in Ref. [37]. For an ideal calibration of our setup, the procedure proposed in Ref. [37] should be followed, but in our case, we will choose a more simple approach. The reason is that for an ideal calibration procedure, the setup being calibrated should be sufficiently sensitive to the isotopic ratio ^{18}r, which is not our case. Moreover, such types of calibration procedures are more suitable when targeting high accuracy and low uncertainty measurements, which is not the purpose of this study. Hence we chose an approach inspired by Ref. [37] but more suitable for our setup.

As with other calibration procedures, ours consists of studying the response of the spectrometer with precharacterized isotopic ratio gas samples of CO_2. Here we used samples originating from two commercially available gas bottles with a known but different $\delta\,^{13}C$ value to improve the consistency of our measurements [38]. To confirm and refine the values given by the manufacturer, several samples from these two bottles were also characterized using an isotope ratio mass spectrometer (Delta V ThermoScientific) giving us the following values $\delta\,^{13}C = (-2.6 \pm 0.1)‰$ and $\delta\,^{13}C = (-24.6 \pm 0.1)‰$, respectively, relatively to the VPDB.

To perform the calibration with our setup, we first fill a 10-cm-long cell with a mixture of 2.5% of CO_2 coming from one precharacterized gas bottle and the rest of synthetic air at a total pressure of 800 mbar. Note that for the calibration procedure and further measurements, we will work at the same partial pressure of CO_2 and at the same total pressure. This is done to avoid any potential pressure dependence of our measurements. One could also calibrate the setup in partial pressure, but this increases the complexity and induces a new potential source of errors. Then, we record the absorption spectrum of the sample in the cell in the same way as detailed before using 20-s-long interferograms. The spectrum is then compared with a fitted spectrum and the $^{13}r_{\text{exp}}$ ratio is extracted from the least-squares regression. A typical example of recorded spectrum is shown in Fig. 4 along with the fitted spectrum used for comparison and the difference between the two sets of data. The same measurement under the same condition is made with the second precharacterized gas bottle. As explained before, the obtained values can be very different from those expected, which is due to the nonperfect response of our setup. However, from the measurements with the two precharacterized gas bottles, we now possess a way of linking the measured $^{13}r_{\text{exp}}$ values with those expected using a calibration equation that we choose as linear.

Once the calibration is done, we can investigate an unknown sample of CO_2 which here will be a gas bottle of unknown $\delta\,^{13}C$ value. In the same condition as in the calibration procedure, we record a transmission spectrum that is compared with a fitted spectrum. From the regression, one can extract the isotopic ratio $^{13}r_{\text{exp}}$ for this gas sample and by applying the inverted calibration equation, we can obtain a $\delta\,^{13}C$ measurement for this sample. The calibration procedure and the measurement using gas samples from the bottle under characterization are repeated several times over several days. The obtained results and their associated error bars, which are given by two times the calibrated standard deviation resulting from the least-squares regression, are presented in Fig. 5.

A simple statistical analysis of the results obtained can give us the mean value and their dispersion which is given

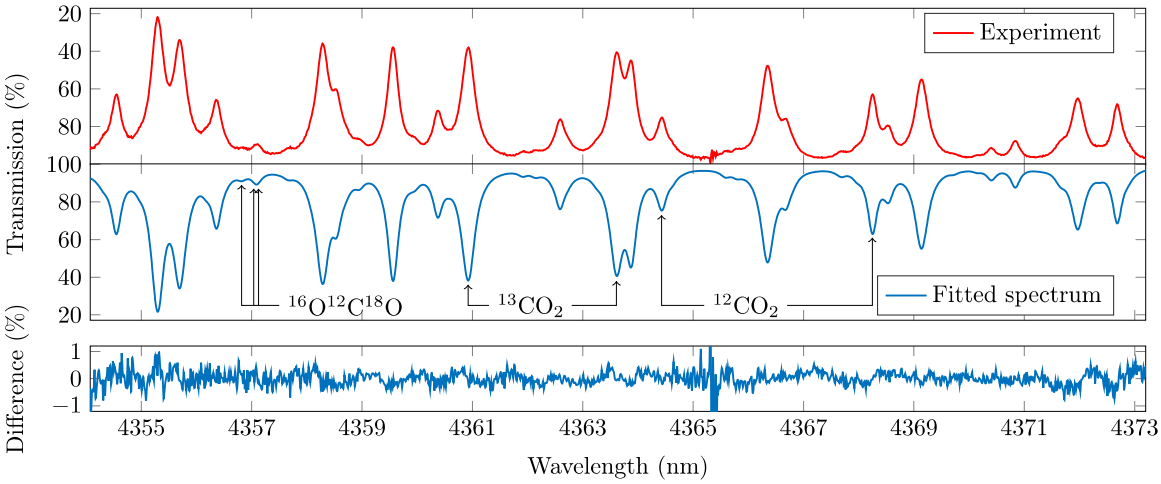

FIG. 4. (Top) Absorption spectrum of a 2.5% CO_2 and 97.5% air gas mixture recorded around 4364 nm at a pressure of 800 mbar using a 20-s-long interferogram. (Middle) Fitted absorption spectrum using line parameters coming from the HITRAN database. (Bottom) Difference between the experimental and the fitted spectra.

by the standard deviation of this whole set of measurements. We found a $\delta\,^{13}C$ value that is

$$\delta\,^{13}C = (-33.2 \pm 1.7)‰.$$

Note that for this measurement set, individual measurements show standard deviation close to 1.1 for half of them and close to 1.8 for the other half. The reason for such differences might be due to the setup stability that can slightly change over the days. The value obtained from the statistical analysis can be compared with a set of measurements made by the isotope ratio mass spectrometer previously used. The result obtained with this instrument is $\delta\,^{13}C = (-34.3 \pm 0.1)‰$, which shows a good agreement within errors with the value given by our isotope ratio dual-comb spectrometer.

2. *Nitrous oxide and* $\delta\,^{15}N^{\alpha}$

Still using the frequency agility of the setup, it is possible to investigate nitrous oxide since absorption bands of this molecule and its isotopologues are present below 5 μm [39].

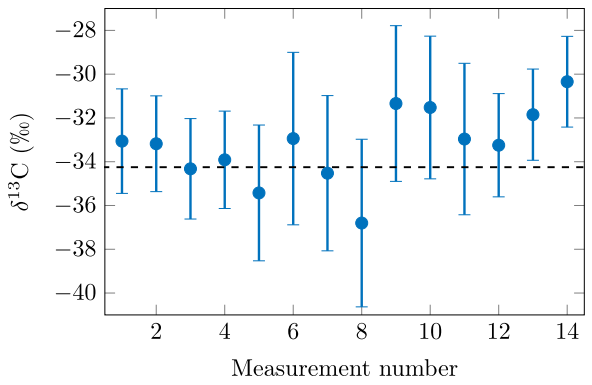

FIG. 5. Graph showing $\delta\,^{13}C$ measurements and their error bars at a confidence level of 95% (2 standard deviations) of gas samples coming a gas bottle under characterization. The dashed line represents a $\delta\,^{13}C$ measurement of the same bottle obtained using an isotope ratio mass spectrometer.

In our case we study the spectral region around 4.63 μm where the nitrous oxide isotopologues $^{14}N_2O$ and $^{14}N\,^{15}NO$ show absorption lines with similar intensities when close to the natural isotopic abundance. Hence in the same way as we did for carbon dioxide and the $\delta\,^{13}C$ measurement, it is possible to perform $\delta\,^{15}N^{\alpha}$ measurements, the upperscript α being used to differentiate $^{14}N\,^{15}NO$ and $^{15}N\,^{14}NO$ due to the fact that they do not show the same absorption features. As shown with the measurement of $\delta\,^{13}C$, a complete measurement of the $\delta\,^{15}N^{\alpha}$ ratio would require a calibration of our spectrometer with precharacterized samples of nitrous oxide in isotopic ratio. Considering we already presented the same study for the measurement of $\delta\,^{13}C$, here we will only present raw uncalibrated measurements to illustrate the features of our setup regarding nitrous oxide studies.

The setup is set with an idler CW laser at 2342 nm, which gives a MIR signal that is centered at 4627 nm. The 10-cm cell is filled with a gas mixture of 10% nitrous oxide and 90% synthetic air at a total pressure of 455 mbar. A 60-s-long interferogram is then recorded and treated as explained previously to recover the absorption spectrum of the gas injected in the cell, and a typical example of obtained spectrum is shown is Fig. 6 (top). As with carbon dioxide, the spectrum is compared with a fitted spectrum obtained by least-squares regression which is shown in Fig. 6 (middle), and the difference between the two sets of data is presented in Fig. 6 (bottom). For the least-squares regression, the model used here is the same as the one used before, which is a set of Voigt profiles with N_2O line parameters given by the HITRAN database, and only the free parameters have been changed to accommodate for the difference of study in isotopic ratios. Several recordings showed a raw standard deviation resulting from the regression around 2, which is slightly above the raw standard deviations obtained in the $^{13}r_{\mathrm{exp}}$ measurements and at the price of a longer interferogram recording. However, it is not possible to give any concrete significance to this value, especially on the measurement uncertainty for the $\delta\,^{15}N^{\alpha}$ ratio as long as the setup is not yet calibrated.

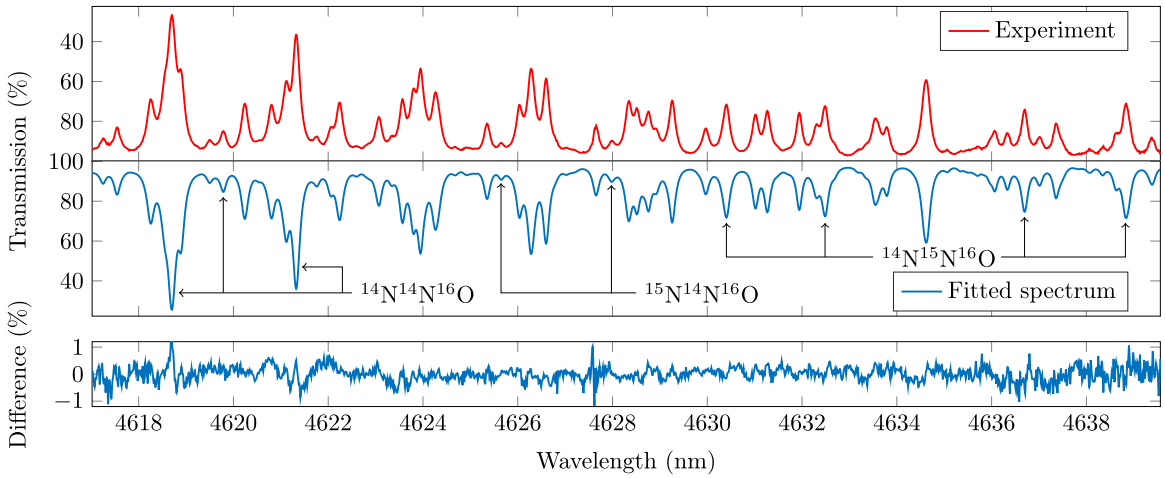

FIG. 6. (Top) Absorption spectrum of a 10% N_2O and 90% air gas mixture recorded around 4628 nm at a total pressure of 455 mbar using a 60-s-long interferogram. (Middle) Fitted absorption spectrum using line parameters coming from the HITRAN database. (Bottom) Difference between the experimental and fitted spectra.

IV. DISCUSSIONS AND CONCLUSION

In this article, we presented a free running dual-comb setup operating in the MIR for IRMs. We showed that by an appropriate choice of the analysis spectral range and by calibrating our setup against precharacterized gas samples, it was possible to accurately measure the relative isotopic ratio $\delta\,^{13}C$ with a standard deviation below 2‰. The measurements performed present a very good repeatability, and a comparison with data obtained using a mass spectrometer showed a very good agreement, thus validating the use of DCS for IRMs. The work presented here, and especially the measurement uncertainties, could be improved by stabilizing against frequency standards the CW lasers used, by decreasing the repetition rates of the combs for a higher spectral resolution, by increasing the spectral windows investigated with a shorter PPLN crystal, or even by using more advanced procedures for data analyses [40]. We believe these potential enhancements could improve the measurements delivered by our setup and thus compete with several isotope ratio spectrometers currently available on the market. However, let us note that the typical uncertainties obtained here can already be enough for several applications, such as for the detection of *Helicobacter pylori* infection by breath test which requires a threshold around 3‰ [41] and even comparable with the precision of embedded spectrometers on martian rovers such as Curiosity, which is around 2‰ [42,43].

Although any dual-comb spectrometer could be used for such IRMs, electro-optic frequency combs seem to be very good candidates for miniaturizing such kinds of setups since they can be generated on-chip [44,45], which could enable easier on field IRMs with embedded systems. Combs generated with microresonators could also be possible candidates for the design of compact dual-comb spectrometers and thus for IRMs [46,47]. Regarding the applications, in the case of carbon IRMs, changes in the absorption length could result in the study of atmospheric conditions or using pure carbon dioxide samples. The first possibility has shown particular interest [48], whereas the second could avoid the use of diluting the samples in air and be particularly useful for applications where a relatively high amount of CO_2 can be used. The technique presented here could in principle also be used to target other molecular species, such as sulfur isotopes via the study of sulfur dioxide [49], but this would require going further in the MIR, above 5 μm where PPLN crystals are no more transparent. However, other materials and techniques were reported for studying such spectral regions [50,51]. To conclude, the results presented here show that DCS has a high potential in the measurement of isotope ratios, and we believe that these results could pave the way to new kinds of isotope ratio spectrometers.

ACKNOWLEDGMENTS

The authors thank Vincent Boudon for his availability to answer many questions related to the HITRAN database and spectroscopy and Ivan Jovovic for his help in running the isotope ratio mass spectrometer measurements. We acknowledge funding from the Centre National de la Recherche Scientifique (CNRS), Conseil Régional de Bourgogne Franche-Comté, iX-Core Research Fondation, Agence Nationale de la Recherche (ANR-19-CE47-0008, ANR-15-IDEX-0003, ANR-21-CE42-0026-01, ANR-21-ESRE-0040).

[1] K. M. Frei, U. Mannering, K. Kristiansen, M. E. Allentoft, A. S. Wilson, I. Skals, S. Tridico, M. Louise Nosch, E. Willerslev, L. Clarke, and R. Frei, Tracing the dynamic life story of a Bronze Age Female, Sci. Rep. **5**, 10431 (2015).

[2] J. Jaubert, S. Verheyden, D. Genty, M. Soulier, H. Cheng, D. Blamart, C. Burlet, H. Camus, S. Delaby, D. Deldicque, R. L. Edwards, C. Ferrier, F. Lacrampe-Cuyaubère, F. Lévêque, F. Maksud, P. Mora, X. Muth, É. Régnier, J.-N. Rouzaud, and

F. Santos, Early Neanderthal constructions deep in Bruniquel Cave in southwestern France, Nature (London) **534**, 111 (2016).

[3] C. R. Webster, P. R. Mahaffy, G. J. Flesch, P. B. Niles, J. H. Jones, L. A. Leshin, S. K. Atreya, J. C. Stern, L. E. Christensen, T. Owen, H. Franz, R. O. Pepin, A. Steele, and the MSL Science Team, Isotope Ratios of H, C, and O in CO_2 and H_2O of the Martian Atmosphere, Science **341**, 260 (2013).

[4] Z. Tian, T. Magna, J. M. D. Day, K. Mezger, E. E. Scherer, K. Lodders, R. C. Hin, P. Koefoed, H. Bloom, and K. Wang, Potassium isotope composition of Mars reveals a mechanism of planetary volatile retention, Proc. Natl. Acad. Sci. USA **118**, e2101155118 (2021).

[5] C. H. House, G. M. Wong, C. R. Webster, G. J. Flesch, H. B. Franz, J. C. Stern, A. Pavlov, S. K. Atreya, J. L. Eigenbrode, A. Gilbert, A. E. Hofmann, M. Millan, A. Steele, D. P. Glavin, C. A. Malespin, and P. R. Mahaffy, Depleted carbon isotope compositions observed at Gale crater, Mars, Proc. Natl. Acad. Sci. USA **119**, e2115651119 (2022).

[6] A. Ruf, B. Kanawati, N. Hertkorn, Q.-Z. Yin, F. Moritz, M. Harir, M. Lucio, B. Michalke, J. Wimpenny, S. Shilobreeva, B. Bronsky, V. Saraykin, Z. Gabelica, R. D. Gougeon, E. Quirico, S. Ralew, T. Jakubowski, H. Haack, M. Gonsior, P. Jenniskens *et al.*, Previously unknown class of metalorganic compounds revealed in meteorites, Proc. Natl. Acad. Sci. USA **114**, 2819 (2017).

[7] R. Tartèse, M. Chaussidon, A. Gurenko, F. Delarue, and F. Robert, Insights into the origin of carbonaceous chondrite organics from their triple oxygen isotope composition, Proc. Natl. Acad. Sci. USA **115**, 8535 (2018).

[8] F. Camin, L. Bontempo, M. Perini, and E. Piasentier, Stable isotope ratio analysis for assessing the authenticity of food of animal origin, Compr. Rev. Food Sci. Food Saf. **15**, 868 (2016).

[9] J. R. Brooks, N. Buchmann, S. Phillips, B. Ehleringer, R. D. Evans, M. Lott, L. A. Martinelli, W. T. Pockman, D. Sandquist, J. P. Sparks, L. Sperry, D. Williams, and J. R. Ehleringer, Heavy and light beer: a carbon isotope approach to detect C_4 Carbon in beers of different origins, styles, and prices, J. Agric. Food Chem. **50**, 6413 (2002).

[10] M. P. Day, B. Zhang, and G. J. Martin, Determination of the geographical origin of wine using joint analysis of elemental and isotopic composition. II—Differentiation of the principal production zones in France for the 1990 vintage, J. Sci. Food Aric. **67**, 113 (1995).

[11] D. A. Magdas, S. Cuna, G. Cristea, R. E. Ionete, and D. Costinel, Stable isotopes determination in some Romanian wines, Isot. Environ. Health Stud. **48**, 345 (2012).

[12] I.-M. Chung, J.-G. Han, W.-S. Kong, J.-K. Kim, M.-J. An, J.-H. Lee, Y.-J. An, M. Y. Jung, and S.-H. Kim, Regional discrimination of Agaricus bisporus mushroom using the natural stable isotope ratios, Food Chem. **264**, 92 (2018).

[13] F. Camin, K. Wietzerbin, A. B. Cortes, G. Haberhauer, M. Lees, and G. Versini, Application of multielement stable isotope ratio analysis to the characterization of french, italian, and spanish cheeses, J. Agric. Food Chem. **52**, 6592 (2004).

[14] D. Y. Graham, D. J. Evans, L. C. Alpert, P. D. Klein, D. G. Evans, A. R. Opekun, and T. W. Boutton, Campylobacter pylori detected noninvasively by the ^{13}C-urea breath test, Lancet **329**, 1174 (1987).

[15] L. Yang, Accurate and precise determination of isotopic ratios by MC-ICP-MS: A review, Mass Spectrom. Rev. **28**, 990 (2009).

[16] E. Kerstel, Chapter 34 - Isotope ratio infrared spectrometry, in *Handbook of Stable Isotope Analytical Techniques*, edited by P. A. de Groot (Elsevier, Amsterdam, 2004), pp. 759–787.

[17] J. F. Becker, T. B. Sauke, and M. Loewenstein, Stable isotope analysis using tunable diode laser spectroscopy, Appl. Opt. **31**, 1921 (1992).

[18] H. Waechter and M. Sigrist, Mid-infrared laser spectroscopic determination of isotope ratios of N_2O at trace levels using wavelength modulation and balanced path length detection, Appl. Phys. B **87**, 539 (2007).

[19] E. H. Wahl, B. Fidric, C. W. Rella, S. Koulikov, B. Kharlamov, S. Tan, A. A. Kachanov, B. A. Richman, E. R. Crosson, B. A. Paldus, S. Kalaskar, and D. R. Bowling, Applications of cavity ring-down spectroscopy to high precision isotope ratio measurement of ^{13}C / ^{12}C in carbon dioxide, Isot. Environ. Health Stud. **42**, 21 (2006).

[20] I. Coddington, N. Newbury, and W. Swann, Dual-comb spectroscopy, Optica **3**, 414 (2016).

[21] T. Fortier and E. Baumann, 20 years of developments in optical frequency comb technology and applications, Commun. Phys. **2**, 153 (2019).

[22] N. Picqué and T. W. Hänsch, Frequency comb spectroscopy, Nat. Photonics **13**, 146 (2019).

[23] A. V. Muraviev, V. O. Smolski, Z. E. Loparo, and K. L. Vodopyanov, Massively parallel sensing of trace molecules and their isotopologues with broadband subharmonic mid-infrared frequency combs, Nat. Photonics **12**, 209 (2018).

[24] K. L. Vodopyanov, Isotopologues detection and quantitative analysis by mid-infrared dual-comb laser spectroscopy, in *Encyclopedia of Analytical Chemistry* (American Cancer Society, 2020), pp. 1–11.

[25] A. Parriaux, K. Hammani, and G. Millot, Electro-optic frequency combs, Adv. Opt. Photonics **12**, 223 (2020).

[26] G. Millot, S. Pitois, M. Yan, T. Hovhannisyan, A. Bendahmane, T. W. Hänsch, and N. Picqué, Frequency-agile dual-comb spectroscopy, Nat. Photonics **10**, 27 (2016).

[27] M. Yan, P.-L. Luo, K. Iwakuni, G. Millot, T. W. Hänsch, and N. Picqué, Mid-infrared dual-comb spectroscopy with electro-optic modulators, Light: Sci. Appl. **6**, e17076 (2017).

[28] A. Parriaux, M. Conforti, A. Bendahmane, J. Fatome, C. Finot, S. Trillo, N. Picqué, and G. Millot, Spectral broadening of picosecond pulses forming dispersive shock waves in optical fibers, Opt. Lett. **42**, 3044 (2017).

[29] B. Jerez, P. Martín-Mateos, F. Walla, C. de Dios, and P. Acedo, Flexible electro-optic, single-crystal difference frequency generation architecture for ultrafast mid-infrared dual-comb spectroscopy, ACS Photonics **5**, 2348 (2018).

[30] P.-L. Luo, E.-C. Horng, and Y.-C. Guan, Fast molecular fingerprinting with a coherent, rapidly tunable dual-comb spectrometer near 3 μm, Phys. Chem. Chem. Phys. **21**, 18400 (2019).

[31] http://www.cfa.harvard.edu/hitran/.

[32] I. Gordon, L. Rothman, R. Hargreaves, R. Hashemi, E. Karlovets, F. Skinner, E. Conway, C. Hill, R. Kochanov, Y. Tan, P. Wcisło, A. Finenko, K. Nelson, P. Bernath, M. Birk, V. Boudon, A. Campargue, K. Chance, A. Coustenis, B. Drouin *et al.*, The HITRAN2020 molecular spectroscopic

database, J. Quant. Spectrosc. Radiat. Transfer **277**, 107949 (2022).

[33] I. Robinson, H. L. Butcher, N. A. Macleod, and D. Weidmann, Hollow waveguide integrated laser spectrometer for $^{13}CO_2/^{12}CO_2$ analysis, Opt. Express **27**, 35670 (2019).

[34] A. L. Sessions, Isotope-ratio detection for gas chromatography, J. Sep. Sci. **29**, 1946 (2006).

[35] International Atomic Energy Agency, *Reference and Intercomparison Materials for Stable Isotopes of Light Elements*, TECDOC Series No. 825 (International Atomic Eenergy Agency, Vienna, 1995).

[36] A. J. Fleisher, H. Yi, A. Srivastava, O. L. Polyansky, N. F. Zobov, and J. T. Hodges, Absolute $^{13}C/^{12}C$ isotope amount ratio for Vienna PeeDee Belemnite from infrared absorption spectroscopy, Nat. Phys. **17**, 889 (2021).

[37] D. W. T. Griffith, Calibration of isotopologue-specific optical trace gas analysers: a practical guide, Atmos. Meas. Tech. **11**, 6189 (2018).

[38] T. B. Coplen, W. A. Brand, M. Gehre, M. Gröning, H. A. J. Meijer, B. Toman, and R. M. Verkouteren, New guidelines for $\delta^{13}C$ measurements, Anal. Chem. **78**, 2439 (2006).

[39] D. M. Bailey, G. Zhao, and A. J. Fleisher, Precision spectroscopy of nitrous oxide isotopocules with a cross-dispersed spectrometer and a mid-infrared frequency comb, Anal. Chem. **92**, 13759 (2020).

[40] A. Castrillo, H. Dinesan, G. Casa, G. Galzerano, P. Laporta, and L. Gianfrani, Amount-ratio determinations of water isotopologues by dual-laser absorption spectrometry, Phys. Rev. A **86**, 052515 (2012).

[41] T. T. Perets, R. Gingold-Belfer, H. Leibovitzh, D. Itskoviz, H. Schmilovitz-Weiss, Y. Snir, R. Dickman, I. Dotan, Z. Levi, and D. Boltin, Optimization of ^{13}C-urea breath test threshold levels for the detection of Helicobacter pylori infection in a national referral laboratory, J. Clin. Lab. Anal. **33**, e22674 (2019).

[42] C. R. Webster and P. R. Mahaffy, Determining the local abundance of Martian methane and its' $^{13}C/^{12}C$ and D/H isotopic ratios for comparison with related gas and soil analysis on the 2011 Mars Science Laboratory (MSL) mission, Planet. Space Sci. **59**, 271 (2011).

[43] P. R. Mahaffy, C. R. Webster, M. Cabane, P. G. Conrad, P. Coll, S. K. Atreya, R. Arvey, M. Barciniak, M. Benna, L. Bleacher, W. B. Brinckerhoff, J. L. Eigenbrode, D. Carignan, M. Cascia, R. A. Chalmers, J. P. Dworkin, T. Errigo, P. Everson, H. Franz, R. Farley *et al.*, The Sample Analysis at Mars Investigation and Instrument Suite, Space Sci. Rev. **170**, 401 (2012).

[44] A. Rueda, F. Sedlmeir, M. Kumari, G. Leuchs, and H. G. L. Schwefel, Resonant electro-optic frequency comb, Nature (London) **568**, 378 (2019).

[45] M. Zhang, B. Buscaino, C. Wang, A. Shams-Ansari, C. Reimer, R. Zhu, J. M. Kahn, and M. Lončar, Broadband electro-optic frequency comb generation in a lithium niobate microring resonator, Nature (London) **568**, 373 (2019).

[46] P. Trocha, M. Karpov, D. Ganin, M. H. P. Pfeiffer, A. Kordts, S. Wolf, J. Krockenberger, P. Marin-Palomo, C. Weimann, S. Randel, W. Freude, T. J. Kippenberg, and C. Koos, Ultrafast optical ranging using microresonator soliton frequency combs, Science **359**, 887 (2018).

[47] G. Lin and Q. Song, Kerr Frequency Comb Interaction with Raman, Brillouin, and Second Order Nonlinear Effects, Laser Photonics Rev. **16**, 2100184 (2022).

[48] D. Nelson, J. McManus, S. Herndon, M. Zahniser, B. Tuzson, and L. Emmenegger, New method for isotopic ratio measurements of atmospheric carbon dioxide using a 4.3μm pulsed quantum cascade laser, Appl. Phys. B **90**, 301 (2008).

[49] L. E. Christensen, B. Brunner, K. N. Truong, R. E. Mielke, C. R. Webster, and M. Coleman, Measurement of sulfur isotope compositions by tunable laser spectroscopy of SO_2, Anal. Chem. **79**, 9261 (2007).

[50] P.-L. Luo, Long-wave mid-infrared time-resolved dual-comb spectroscopy of short-lived intermediates, Opt. Lett. **45**, 6791 (2020).

[51] A. S. Kowligy, D. R. Carlson, D. D. Hickstein, H. Timmers, A. J. Lind, P. G. Schunemann, S. B. Papp, and S. A. Diddams, Mid-infrared frequency combs at 10 GHz, Opt. Lett. **45**, 3677 (2020).